Electronic Supplementary Material (ESI) for Lab on a Chip.

Supporting Information "Scalable production of double emulsion with thin shells"

Antoine Vian[1], Baptiste Reuse[1] and Esther Amstad[1]

[1] Soft Materials Laboratory, Institute of Materials, École Polytechnique Fédérale de Lausanne, 1015 Lausanne, Switzerland

Quantification of the shell thickness

We cannot quantify the shell thickness directly from optical microscopy images of double emulsions because it is at or below the resolution limit. To quantify the shell thickness, we measure the outer radius of the double emulsion drop, R_0, using optical microscopy. We subsequently rupture the drop by adding isopropanol to the outer phase and measure the radius of the resulting oil drop, r.[1] By volume conservation we obtain:

$$\frac{4}{3}\pi {R_0}^3 - \frac{4}{3}\pi (R_0 - d)^3 = \frac{4}{3}\pi r^3$$

such that the shell thickness, d, is defined as:

$d = R_0 - ({R_0}^3 - r^3)^{\frac{1}{3}}$.

To test the accuracy of this method, we employed it to quantify the shell thickness of double emulsions with thick shells and compared these values with results obtained from direct optical microscopy images. Moreover, we compared these results to values obtained from optical microscopy images of compressed double emulsions, as has previously been reported.[1–5] The values obtained from all these different measurement methods are in good agreement, suggesting that the use of isopropanol to rupture drops does not introduce systematic measurement errors.[1]

Accuracy of the measurment for the drop radius

To quantify the drop radius, we acquire images with pixel sizes of 0.5×0.5 μm^2 such that the resolution limit on these images is 1 μm. To increase the accuracy of our measurements, we quantify the total area, A, of the drops and obtain a measurement error of the area of $\Delta A \approx 1$ μm^2.

We calculate the upper and lower limit of the drop area, A^+, and A^- using:

$A^+ = \pi(R_0 + \Delta R)^2$ and $A^+ = \pi(R_0 - \Delta R)^2$; here R_0 is the mean radius (around 50 μm) and ΔR the given error of the measurment. Hence, we obtain:

$$A^+ - A^- = 2\Delta A = \pi[(R_0 + \Delta R)^2 - (R_0 - \Delta R)^2]$$

$$\Rightarrow \quad 2\Delta A = \pi {R_0}^2 \left[(1 + \tfrac{\Delta R}{R_0})^2 - (1 - \tfrac{\Delta R}{R_0})^2\right]$$

$$\Rightarrow \quad 2\Delta A = \pi R^2 \left[(1 + 2\tfrac{\Delta R}{R_0} + \left(\tfrac{\Delta R}{R_0}\right)^2) - (1 - 2\tfrac{\Delta R}{R_0} + \left(\tfrac{\Delta R}{R_0}\right)^2)\right]$$

$$\Rightarrow \quad 2\Delta A = 4\pi {R_0}^2 \left[\tfrac{\Delta R}{R_0}\right]$$

$$\Rightarrow \quad \Delta R = \tfrac{1}{2\pi}\left[\tfrac{\Delta A}{R_0}\right]$$

$$\boxed{\Rightarrow \quad \Delta R \approx 0.05\ \mu\text{m}}$$

Hence, using this technique, we can obtain a resolution of 0.1 μm instead of 1 μm that is achieved through a direct quantification from optical micrographs.

Accuracy of the shell thickness measurment

Using optical microscopy images and volume conservation, we determine the shell thickness, d, as detailed above using :

$d = R_0 - ({R_0}^3 - r^3)^{\frac{1}{3}}$.

The largest error in quantifying d comes from the measurement of R_0. To determine this error, we quantify an upper and lower limit for the shell thickness d^+ and d^-, by adding and subtracting the measurement error of R_0, ΔR:

$d^+ = R_0 + \Delta R - [(R_0 + \Delta R)^3 - r^3)]^{\frac{1}{3}}$.

$d^- = R_0 - \Delta R - [(R_0 - \Delta R)^3 - r^3)]^{\frac{1}{3}}$.

Hence the maximum error on the measurement for the shell thickness is determined by :

$\Delta d = d^{+} - d^{-} = 2\Delta R - [(R_0 + \Delta R)^3 - r^3)]^{\frac{1}{3}} - [(R_0 - \Delta R)^3 - r^3)]^{\frac{1}{3}}$

⇨ $\Delta d = 2\Delta R - R_0 \left\{ \left[\left(1 + \frac{\Delta R}{R_0}\right)^3 - \left(\frac{r}{R_0}\right)^3 \right]^{\frac{1}{3}} - \left[\left(1 - \frac{\Delta R}{R_0}\right)^3 - \left(\frac{r}{R_0}\right)^3 \right]^{\frac{1}{3}} \right\}$

⇨ $\Delta d = 2\Delta R - R_0 \left\{ \left[1 + 3\frac{\Delta R}{R_0} + 3\left(\frac{\Delta R}{R_0}\right)^2 + \left(\frac{\Delta R}{R_0}\right)^3 - \left(\frac{r}{R_0}\right)^3 \right]^{\frac{1}{3}} - \left[1 - 3\frac{\Delta R}{R_0} + 3\left(\frac{\Delta R}{R_0}\right)^2 - \left(\frac{\Delta R}{R_0}\right)^3 - \left(\frac{r}{R_0}\right)^3 \right]^{\frac{1}{3}} \right\}$

If we consider $\frac{\Delta R}{R_0} \ll 1$ and $\left(\frac{r}{R_0}\right)^3 \ll 1$ we can simplify the formula:

⇨ $\Delta d = 2\Delta R - R_0 \left\{ \left[1 - \left(\frac{r}{R_0}\right)^3 + \frac{1}{3}\left(3\frac{\Delta R}{R_0} + 3\left(\frac{\Delta R}{R_0}\right)^2 + \left(\frac{\Delta R}{R_0}\right)^3\right) \right] - \left[1 - \left(\frac{r}{R_0}\right)^3 + \frac{1}{3}\left(-3\frac{\Delta R}{R_0} + 3\left(\frac{\Delta R}{R_0}\right)^2 - \left(\frac{\Delta R}{R_0}\right)^3\right) \right] + \theta\left(\left(\frac{\Delta R}{R_0}\right)^3\right) \right\}$

⇨ $\Delta d = 2\Delta R - R_0 \left\{ 2\frac{\Delta R}{R_0} + 2\left(\frac{\Delta R}{R_0}\right)^3 + \theta\left(\left(\frac{\Delta R}{R_0}\right)^3\right) \right\}$

⇨ $\Delta d = -2\left(\frac{\Delta R}{R_0}\right)^3 + \theta\left(\left(\frac{\Delta R}{R_0}\right)^3\right)$

In our case, double emulsions with thin shells typically have dimensions of $R_0 \approx 50$ µm, $\Delta R \approx 1$ µm and r $\approx$ 15 µm. Hence the assumptions $\frac{\Delta R}{R_0} \approx 0.02 \ll 1$ and $\left(\frac{r}{R_0}\right)^3 \approx 0.06 \ll 1$ hold and we obtain $\boxed{\Delta d \approx 2\ nm}$.

Hydrodynamic resistances in the aspiration device

To test the influence of the hydrodynamic resistance of the main channel downstream the flow focusing junction on that of the main channel in the aspiration section, we compare the two hydrodynamic resistances:

$R = \left[\frac{12\mu L}{1-0.63\left(\frac{h}{w}\right)}\right]\frac{1}{wh^3}$;

here μ is the dynamic viscosity of the fluid, L the length of the channel, w its width, and h its height. Hence for two equally long channels that are filled with the identical fluid but have different heights, $h_1 = h_2 = 80$ µm and widths, $w_1 = 60$ and $w_1 = 180$ µm, and therefore different hydrodynamic resistances R_1 and R_2 we obtain:

$$\frac{R_1}{R_2} = \left[\frac{1 - 0.63\left(\frac{h_2}{w_2}\right)}{1 - 0.63\left(\frac{h_1}{w_1}\right)}\right]\frac{w_2 {h_2}^3}{w_1 {h_1}^3} = 5.6$$

Influence of the outer Flow Rate

To spatially separate the double emulsions that are jammed in the aspiration section in the final parts of the aspiration device, we introduce an aqueous phase downstream the aspiration section. This outer phase is injected at a rate, Q_o. To test the influence of Q_o on the shell thickness of processed double emulsions, we vary Q_o from 300 µL/h to 6000 µL/h and keep the injection and withdraw flow rates constant at Q_i = 1000 µL/h and Q_w = 800 µL/h. Our results demonstrate that the shell thickness of processed double emulsions is independent of the flow rate of the outer fluid, Q_o, as shown in Figure S1.

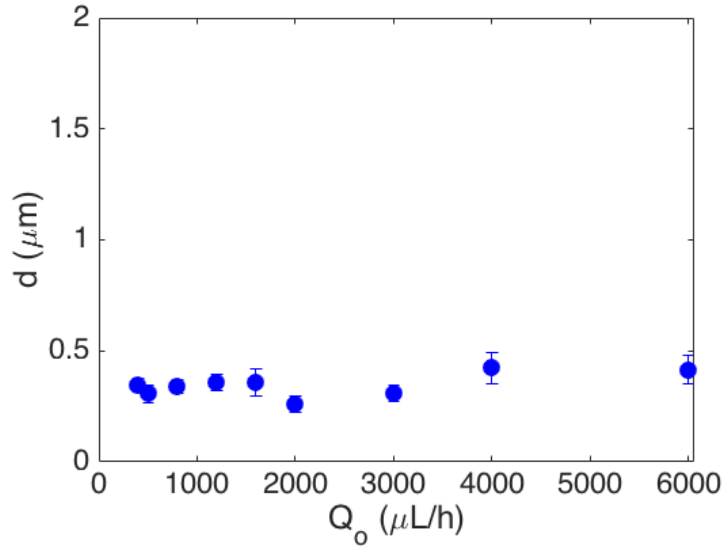

Figure S1: Shell thickness, *d*, of processed double emulsion drops as a function of the injection flow rate for the outermost aqueous phase, $\boldsymbol{Q_o}$. The injection rate for the double emulsions and the withdraw rate are kept constant at $\boldsymbol{Q_i}$ = 1000 µL/h and $\boldsymbol{Q_w}$ = 800 µL/h.

Estimation of the pressure profile in the main channel

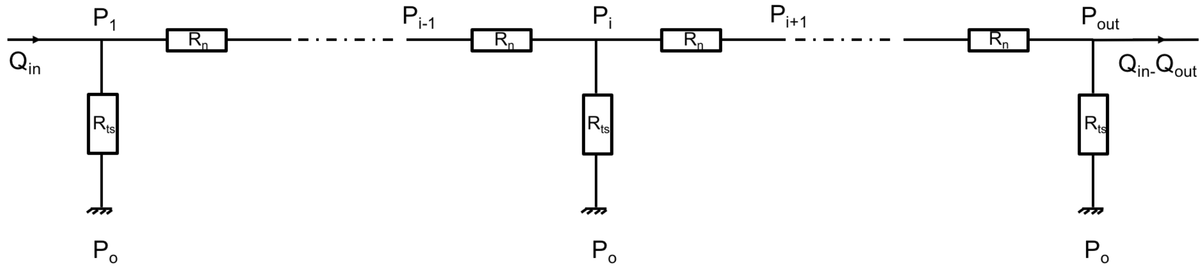

Figure S2: Schematic illustration of the electric circuit analogue used to estimate the pressure profile within the channels. $\boldsymbol{R_n}$ corresponds to the hydrodynamic resistance in the main channel between each shunt channel and $\boldsymbol{R_{ts}}$ is the resistance associated with each pair of shunt channel.

To estimate the pressure profile within the main channel, we employ an electric circuit analogue, as schematically shown in Figure S2. Because all the shunt channels lead into one of the two large reservoirs and the two reservoirs are connected to each other, we approximate the pressure at the end of each shunt channel to be the same, P_o. Moreover, we approximate the resistance of the main channel in each section between adjacent junctions to be R_n. The length of the shunt channels varies from 80 to 200 µm. Nevertheless, to simplify the model, we approximate hydrodynamic resistances of all shunt channels to be equal to R_s corresponding to a length of 100 µm. Within the aspiration section, pairs of shunt channels intersect the main channel at opposite sites, as shown in Figures 1B and 1C. We describe this pair of shunt channels with parallel resistances $\frac{1}{R_{ts}} = \frac{1}{R_s} + \frac{1}{R_s} = \frac{2}{R_s}$, where R_{ts} is the total resistance of the shunt channels at any given junction. At each junction, we apply the node law to relate the different pressures in the channels that lead into this junction. For example, at junction k we obtain:

$$P_k\left(\frac{2}{R_n} + \frac{1}{R_{ts}}\right) - \frac{P_{k-1}+P_{i+1}}{R_n} = \frac{P_o}{R_{ts}}$$

where P_k is the pressure in junction k, P_{k+1} the pressure in junction k+1, P_{k-1} the pressure in junction k-1. We quantify the pressure differences between the different channel sections and therefore set $P_o = 0$ as a basepoint. We write this node equation for each node and obtain n equations with n unknown variables. The boundary conditions are determined by the injection and withdraw rates. Therefore, we can relate the injection rate, Q_i and the withdraw rate Q_i-Q_w to the pressure profile in the main channel using:

$$A.P = Q$$

$$\begin{bmatrix} \left(\frac{1}{R_n}+\frac{1}{R_{ts}}\right) & -1/R_n & 0 & \cdots & 0 \\ -1/R_n & \left(\frac{2}{R_n}+\frac{1}{R_{ts}}\right) & \ddots & \ddots & \vdots \\ 0 & \ddots & \ddots & \ddots & 0 \\ \vdots & \ddots & \ddots & \left(\frac{2}{R_n}+\frac{1}{R_{ts}}\right) & -1/R_n \\ 0 & \cdots & 0 & -1/R_n & \left(\frac{1}{R_n}+\frac{1}{R_{ts}}\right) \end{bmatrix} . \begin{pmatrix} P_1 \\ P_2 \\ \vdots \\ \vdots \\ \vdots \\ P_{n-1} \\ P_n \end{pmatrix} = \begin{pmatrix} Q_{in} \\ 0 \\ \vdots \\ \vdots \\ \vdots \\ 0 \\ Q_{in}-Q_{out} \end{pmatrix}$$

In this case, the matrix is invertible because its determinant is not equal to zero. Hence, we can calculate the pressure profile in the channel by inverting matrix A:

$$P = A^{-1}.Q$$

Using this equation, we obtain the pressure profile throughout the channel at each junction i. The pressure obtained is always relative to the pressure in the reservoir at the output of the shunt channel that is arbitrarily set to 0.
We convert the pressure profile into a flow rate profile inside the main channel using:

$$Q_k = \frac{P_{k+1} - P_k}{R_n}$$

The pressure drops rapidly in the initial parts of the aspiration section and levels off thereafter, as shown in Figure S3A. As a result, the flow rate in the aspiration section also decreases rapidly upstream the junction where the 15th shunt channel intersects the main channel and decreases more slowly thereafter, as shown in Figure S3B. Note, that this profile is obtained for a continuous flow that does not encompass any drops. When drops are present in the main channel, they strongly increase the resistance of the main channel[6] such that we expect the actual pressure decrease in the main channel to be much higher than what is estimated in Figure S3A. However, we do not expect the drops to strongly influence the shape of the pressure profile.

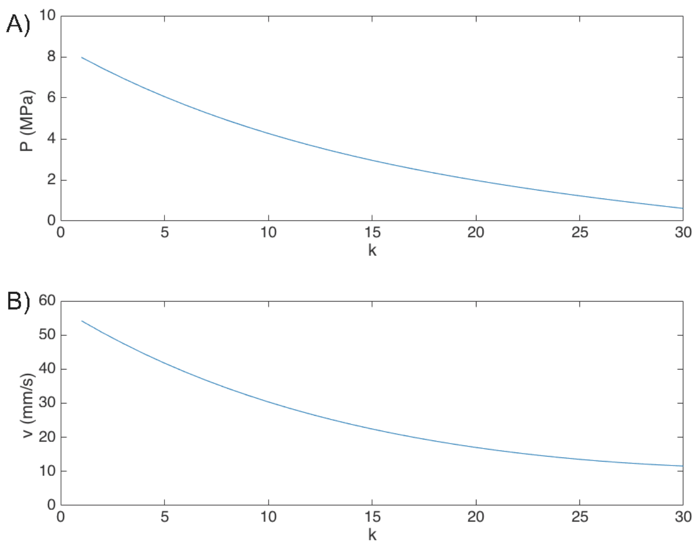

Figure S3: (A) Pressure profile along the main channel, P, as a function of the location measured as the number shunt channel, that are upstream the location of interest, $\boldsymbol{k}$. (B) Velocity profile for a continuous fluid, $\boldsymbol{v}$, derived from the calculated pressure profile as a function of the number of shunts channels located upstream the location of interest, $\boldsymbol{k}$. For these calculations, we fixed $\boldsymbol{Q_i}$ at 1000 µL/h and $\boldsymbol{Q_w}$ at 800 µL/h.

From our model, we can deduce the pressure profile in the channel as a function of Q_i and Q_w. If ΔQ = 300 µL/h is kept constant and Q_i is varied between 1000 µL/h and 2000 µL/h, the pressure at the beginning of the channel depends on Q_i. By contrast, the pressure at the end of the aspiration section is nearly independent of Q_i, as seen in Figure S4A. If Q_i = 1000 µL/h but ΔQ is varied between 100 µL/h and 400 µL/h, the pressure in the initial parts of the aspiration section is very similar whereas the pressure in the final parts of the aspiration section increases with decreasing ΔQ, as seen in Figure S4B.

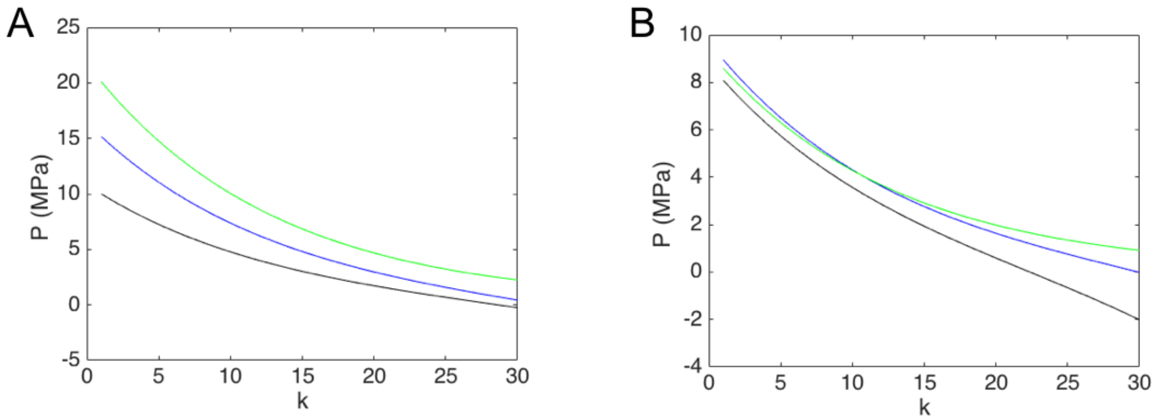

Figure S4: (A) The pressure in the main channel, $\boldsymbol{P}$, as a function of the location the number of shunt channels located upstream the location of interest, **k**, if $\Delta \boldsymbol{Q}$ = 300 µL/h and $\boldsymbol{Q_i}$ = 1000 µL/h (black), 1500 µL/h (blue) and 2000 µL/h (green). (B) The pressure in the main channel, $\boldsymbol{P}$, as a function of the location, **k**, for $\boldsymbol{Q_i}$ = 1000 µL/h and $\Delta \boldsymbol{Q}$ = 400 µL/h (black), 200 µL/h (blue) and 100 µL/h (green)

Quanfitication of drop velocity in the main channel

To test the validity of the calculated flow profile, we measure the velocity of the drops in the main channel as a function of their location using time-lapse optical microscopy images acquired with a high speed camera operated at 3000 frames per second, as exemplified in Figure S5.

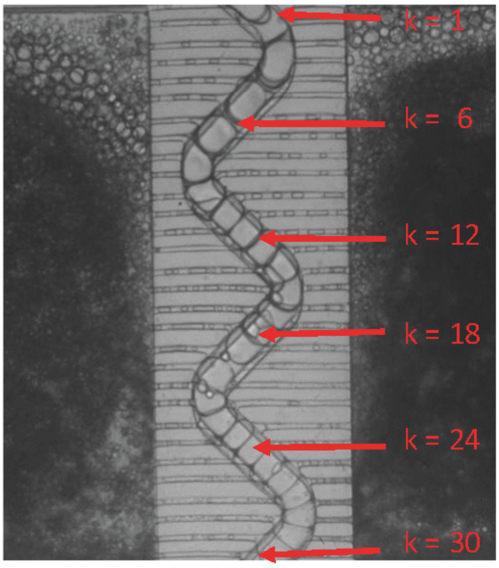

Figure S5: Optical micrograph of the aspiration section in operation with the points between which the average velocity of drops was quantified.

Double emulsions with liquid crystal shells

To test the versatilty of our device, we produce water-oil-water double emulsions with liquid crystal shells and process them using the aspiration device. Also in this case, the aspiration device significantly reduces the shell thickness from 5.7 µm to 1.2 µm, as shown in Figure S6.

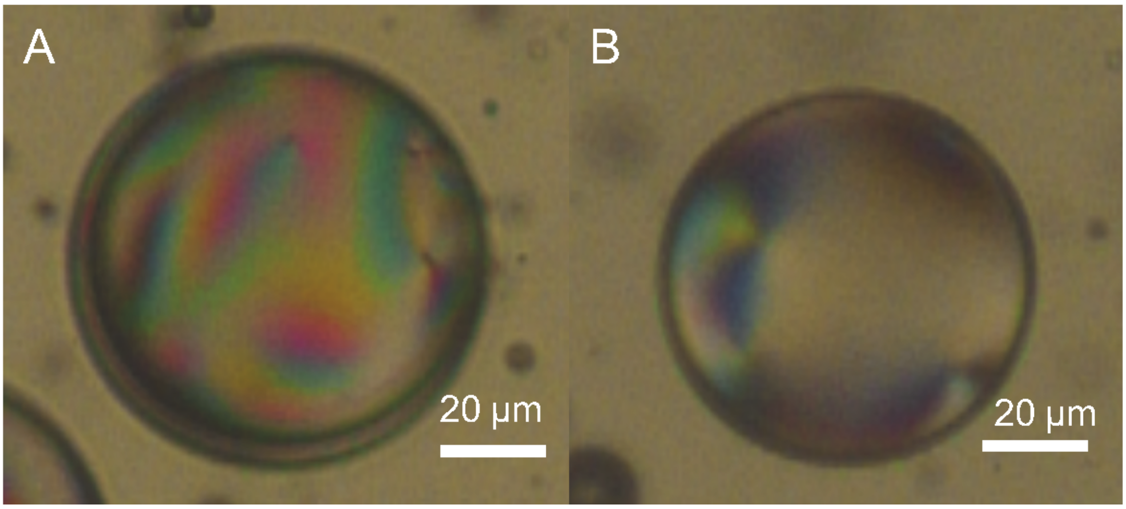

Figure S6: Optical micrographs acquired with polarized light of water-oil-water double emulsions where the oil is a liquid crystal (A) before they are processed where $\boldsymbol{d}$ = 5.70 ± 0.49 µm and (B) after having been processed where $\boldsymbol{d}$ = 1.20 ± 0.21 µm.

Movie S1: Processing of double emulsions with the aspiration device where $\boldsymbol{Q_i}$ = 1000 µL/h , $\boldsymbol{Q_w}$ = 800 µL/h and $\boldsymbol{Q_0}$ = 800 µL/h. The movie is 600 times slowed down.

Movie S2: Operation of the aspiration device in the grey area where $\boldsymbol{Q_w} > \boldsymbol{Q_i}$. The majority of drops flows through the shunt channels and breaks into many much smaller drops at their exit. This operation mode resembles and extrusion of vesicles. The movie is 600 times slowed down.

Movie S3: Operation of the aspiration device in the red area where it does not properly operate such that the shell thicknesses of processed double emulsions are polydisperse. The device is operated at $\boldsymbol{Q_i}$ = 1000 µL/h, $\boldsymbol{Q_w}$ = 1200 µL/h and $\boldsymbol{Q_0}$ = 800 µL/h. Because $\Delta\boldsymbol{Q}$ < 0 µL/h, oil that has been removed from the double emulsions in the initial parts of the aspiration section is re-injected into the main channel further downstream, resulting in a broadening of the shell thicknesses. The movie is 600 times slowed down.

Movie S4: Processing of water-oil-water double emulsions where the oil is oleic acid. The double emulsions are injected at $\boldsymbol{Q_i}$ = 1000 µL/h , $\boldsymbol{Q_w}$ = 800 µL/h and $\boldsymbol{Q_0}$ = 800 µL/h. The movie is 600 times slowed down.

REFERENCES

1 A. Vian, V. Favrod and E. Amstad, *Microfluid. Nanofluidics*, 2016, **20**, 1-9.
2 A. S. Chaurasia, D. N. Josephides and S. Sajjadi, *ChemPhysChem*, 2015, **16**, 403-411.
3 S.-H. Kim, J. W. Kim, J.-C. Cho and D. a Weitz, *Lab Chip*, 2011, **11**, 3162-3166.
4 C. X. Zhao, D. Chen, Y. Hui, D. A. Weitz and A. P. J. Middelberg, *ChemPhysChem*, 2017, **18**, 1393-1399.
5 L. R. Arriaga, E. Amstad and D. a. Weitz, *Lab Chip*, 2015, **10**, 950-956.
6 P. Sajeesh, M. Doble and a. K. Sen, *Biomicrofluidics*, 2014, **8**, 54112.